Mon. Not. R. Astron. Soc. **000**, 000–000 (1999)

Source of excitation of low-l solar p modes: characteristics and solar-cycle variations

W. J. Chaplin[1,2⋆], T. Appourchaux[1], Y. Elsworth[2], G. R. Isaak[2]
B. A. Miller[2] and R. New[3]
[1] *ESA Space Science Department, Solar System Division, ESTEC, 2200 AG Noordwijk, The Netherlands.*
[2] *School of Physics and Astronomy, University of Birmingham, Edgbaston, Birmingham B15 2TT, U.K.*
[3] *School of Science & Mathematics, Sheffield Hallam University, Sheffield S1 1WB*

4 August 1999

ABSTRACT

We investigate various properties of the excitation source that is responsible for driving the acoustic p-mode oscillations of the Sun. Current prejudice places this in the superadiabatic layer of the convection zone. We consider in detail how the precise nature of the resonant mode spectrum is modified: (i) as a result of the impact of different source-multipole mixtures; and (ii) as a function of the radial extent of the source. To do this, we model the observed resonant spectra with the solutions to a simple, one-dimensional wave equation which is intended to describe the essential elements of the solar resonant acoustic cavity. Further, we also fit these models to the low-l peaks in a high-resolution power spectrum generated from data collected by the Birmingham Solar-Oscillations Network (BiSON). We also use the extensive BiSON dataset to search for variations in the source characteristics over the solar cycle.

Key words:
Sun: oscillations – convection – Sun: granulation – Sun: activity – methods: data analysis

1 INTRODUCTION

The high quality of modern helioseismic observations are demanding that greater attention be paid to the more-subtle features now being uncovered in these data. An increasing quantity of recent literature has been devoted to the issue of the now-apparent complex characteristics of the observed resonant p-mode profiles. This body of research has stressed the importance of fitting the modes to models which better reflect this degree of complexity, i.e., in order to obtain reliable estimates of many of the p-mode parameters, a simple Lorentzian no longer suffices (e.g., see Fröhlich et al. 1997; Rhodes et al. 1997; Appourchaux et al. 1998; Korzennik 1998; Rosenthal 1998a, b; Christensen-Dalsgaard et al. 1998; Toutain et al. 1998; and Chaplin et al. 1999); further, it has also made use of the additional information that is contained in the complex resonant forms in order to shed light on the mechanism responsible for exciting the modes (e.g., Duvall et al. 1993; Kumar 1994; Gabriel 1995; Roxburgh & Vorontsov 1995, 1997; Abrams & Kumar 1996; Rast & Bogdan 1998; Nigam et al. 1998; Nigam & Kosovichev 1998, 1999a, b; Kumar & Basu 1999a, b; Chaplin & Appourchaux 1999). In this paper we pay attention to the latter, and build upon the work of Chaplin & Appourchaux.

Chaplin & Appourchaux fitted models based upon the resonant solutions of a one-dimensional acoustic potential to low-angular degree (low-l) p-mode spectra. The resonances of this simple cavity were assumed to be excited by a rudimentary single-multipole source described by a δ function in the radial direction; the fitting extracted direct estimates of the location of the source with respect to the upper turning point (UTP) of the bounded cavity.

They applied these techniques to Doppler velocity observations, under the assumption that such data are uncorrupted by that "correlated" component of the convective granulation that is assumed to be responsible for the reversal in asymmetry of the mode profiles when intensity data are used. Here, we wish to concentrate on the properties of the source, and so model and also fit Doppler velocity data. We have used full-disc, low-l data collected by the ground-based Birmingham Solar-Oscillations Network (BiSON). In particular, we consider: the impact of introducing a source that consists of a mixture of different multipoles; giving the source an extended profile in the radial direction; and possible changes to the source characteristics over the solar activity cycle. However, we begin with a brief recapitulation of

⋆ e-mail: wjc@bison.ph.bham.ac.uk

the cavity model description. (See Abrams & Kumar 1996; Kumar & Basu 1999a; Chaplin & Appourchaux 1999 for the implementation used here.)

2 DESCRIPTION OF THE MODES

The solar acoustic cavity is defined in the form of a rectangular potential well, $\Phi(r)$, of width r_a. $\Phi(r)$ takes infinite values beneath the lower turning point of the cavity (which is located at radius $r = 0$) and a constant, finite value above the UTP (at $r = r_a$). The wave equation describing this system takes the form:

$$\frac{d^2}{dr^2}\Psi + [\omega^2 + i\Gamma\omega - \Phi(r)]\Psi = A_{\rm s}\frac{d^p}{dr^p}\delta(r - r_s). \quad (1)$$

In the above: Ψ is proportional to the Lagrangian pressure perturbation; Γ measures the damping rate; and the system is excited by a δ-function source with amplitude $A_{\rm s}$ located at radius $r = r_s$, where p is an integer which controls the source type. For convenience, we also define the location of the source with respect to the bounded cavity according to $d_s = r_s - r_a$. All radii in the above are defined in seconds of travel time. We seek solutions to Equation 1 under the assumption that the observation height coincides with the top of the cavity – this does not bear on the results of the paper (see Chaplin & Appourchaux for a discussion of this point).

The resonant response of the system to a sudden impulse when $p = 0$ is just the Green's function, G_Ψ, of Equation 1. When $p = 1$ we recover its first derivative dG_Ψ/dr. The function G_Ψ, or a suitable linear combination of it and its derivatives, provides the complex description of the resonant mode profiles that we seek. When d_s is negative, i.e., for the source inside the cavity, one derives (e.g., Abrams & Kumar 1996):

$$G^{\rm in}_\Psi(\omega_1) = -\frac{\sin(\omega_1 r_s)}{\omega_1\cos(\omega_1 r_a) + \omega_2\sin(\omega_1 r_a)}, \quad (2)$$

where $\omega_1^2 = (\omega^2 + i\omega\Gamma)^2$ and $\omega_2^2 = \omega_c^2 - \omega_1^2$. We have set $\nu_c = \omega_c/2\pi$, the acoustic cut-off frequency, to 5.5 mHz throughout our analyses. With the source located outside the cavity (i.e., for d_s positive) we have (Kumar & Basu 1999a):

$$\begin{aligned} G^{\rm out}_\Psi(\omega_1) \quad = \quad & -\frac{\omega_2\sin(\omega_1 r_a)\cosh(\omega_2 d_s)}{\omega_2[\omega_1\cos(\omega_1 r_a) + \omega_2\sin(\omega_1 r_a)]} \\ & -\frac{\omega_1\cos(\omega_1 r_a)\sinh(\omega_2 d_s)}{\omega_2[\omega_1\cos(\omega_1 r_a) + \omega_2\sin(\omega_1 r_a)]}. \end{aligned} \quad (3)$$

We then establish a composite solution across the UTP at $d_s = 0$ (when $r_s = r_a$):

$$G_\Psi = \begin{cases} G^{\rm in}_\Psi & \text{for } d_s \le 0 \\ G^{\rm out}_\Psi & \text{for } d_s > 0 \end{cases} \quad (4)$$

The profiles generated by other source multipoles are just the derivatives of G_Ψ. Here, we consider the first derivatives, which are:

$$\frac{dG^{\rm in}_\Psi(\omega_1)}{dr} = -\frac{\omega_1\cos(\omega_1 r_s)}{\omega_1\cos(\omega_1 r_a) + \omega_2\sin(\omega_1 r_a)}, \quad (5)$$

$$\begin{aligned} \frac{dG^{\rm out}_\Psi(\omega_1)}{dr} \quad = \quad & -\frac{\omega_2\sin(\omega_1 r_a)\sinh(\omega_2 d_s)}{[\omega_1\cos(\omega_1 r_a) + \omega_2\sin(\omega_1 r_a)]} \\ & -\frac{\omega_1\cos(\omega_1 r_a)\cosh(\omega_2 d_s)}{[\omega_1\cos(\omega_1 r_a) + \omega_2\sin(\omega_1 r_a)]}. \end{aligned} \quad (6)$$

We can then establish a composite solution, dG_Ψ/dr (as for G_Ψ in Equation 4) from Equations 5 and 6.

Throughout, we shall consider mode profiles described not only by G_Ψ or dG_Ψ/dr individually, but also by linear combinations of both. Here, we note that all functions are first re-normalized by their maximum values, which we denote by $\widetilde{G}_\Psi$ and $(\widetilde{dG_\Psi/dr})$. Composite profiles made from the linear combination of the re-normalized zeroth and first derivative source terms are denoted by $\mathcal{S}_\Psi$.

Our chief concern is a thorough study of the influence of the source characteristics on the observed forms of the resonant mode profiles. As such, we wish to avoid the added complication of the influence of phenomena distinct from the modes themselves. We have in mind here that component of the convective motion (which excites the acoustic resonances) that is assumed to imprint itself upon observations of the modes and in so doing to modify the shapes of the observed profiles. In the mathematical parlance of our equations above, this corresponds to the complex addition to $\mathcal{S}_\Psi$ of some component which shifts the "zero points" of its real part. This mechanism was first proposed by Roxburgh & Vorontsov (1997) and Nigam et al. (1998) as a means of explaining the opposite signs of asymmetry usually observed in spectra generated from Doppler velocity or intensity observations.

The effect of correlated "noise" has been considered in detail by Nigam & Kosovichev (1999a, b), Kumar & Basu (1999a) and Chaplin & Appourchaux (1999). In these studies, it is assumed that the contaminating influence of the granular motion is far-less severe in the Doppler velocity case (see Chaplin & Appourchaux for a discussion of this point); here, we follow this convention and assume that the velocity data are in fact "uncorrupted". In a power spectrum free from correlated background noise, this would imply that the observed form of the spectrum in the vicinity of a single resonance is determined solely by the interaction of the source characteristics (i.e., location, spatial properties, multipole type) with those of the cavity describing the modal component in question (i.e., size, radial overtone number, damping constant). The presence of uncorrelated background can be suitably corrected or allowed for. The analyses and simulations presented in this paper are therefore of, or relevant to, Doppler velocity data; the contribution of individual resonances to each of our observed (BiSON) or modelled power spectra are then assumed to take the form:

$$P_{\mathcal{S}_\Psi}(\omega) = A^2_{\rm Dopp}\cdot|\mathcal{S}_\Psi|^2, \quad (7)$$

where again $\mathcal{S}_\Psi$ is normalized by its maximum value, and $A_{\rm Dopp}$ is the associated observed amplitude of the mode.

3 EFFECT OF MIXED-MULTIPOLE SOURCE

3.1 Background and context

The acoustic field generated by a particular source distribution can be decomposed into contributions from different multipoles: these can be made from the Green's function G_Ψ and its derivatives. The generation of acoustic noise by turbulent motions was first outlined by Lighthill (1952), and expanded upon for the solar case by, for example, Goldreich & Kumar (1990). The relative contribution of different multipole terms to the excitation of solar p modes is still an open issue, largely owing to the current lack of a complete theory of convection.

Chaplin & Appourchaux considered profiles constructed by either G_Ψ, or its first derivative, dG_Ψ/dr, and fitted these to the low-l mode peaks in a long BiSON spectrum over the range $1800 \leq \nu \leq 4000\,\mu$Hz. They found that in order to match the observed resonances, profiles generated from the first (odd) derivative required a deeper mean source location (~ -1500 km)† than those made from the zeroth (even) derivative (~ -221 km). Further, they also found evidence for a slight frequency-dependence, with lower-frequency modes requiring a deeper source. This is what one might expect from the stratification of eddy scales with height in the atmosphere (e.g., see Abrams & Kumar 1996).

Kumar & Basu (1999b) compared medium-l MDI mode peaks of frequency $\sim 2200\,\mu$Hz to modelled peaks also generated from either G_Ψ or dG_Ψ/dr, and found a very similar source-depth dependence to Chaplin & Appourchaux. From the consideration of other modes, they also uncovered suggestions of a slight dependence with n.

Kumar (1994) inferred a shallow source depth (~ -140 km) by matching profiles based on the first derivative of the Green's function of a set of non-adiabatic inhomogeneous wave equations to observed high-frequency pseudo modes in the range $5300 \leq \nu \leq 7500\,\mu$Hz; further, he found a less satisfactory level of agreement with a source based on the Green's function itself.

Nigam & Kosovichev (1999b) constructed various "solar" sources from combinations of the zeroth, first and second derivatives, weighting the relative contributions according to calculations from a solar model. They compared these with an $l = 200$ MDI spectrum over an extended range of frequencies, and concluded that a source constructed from G_Ψ alone, and located some 75 km beneath the photosphere, provided the most satisfactory match to the observations.

Before proceeding, we note cautiously that it is not necessarily clear the extent to which analyses of the type discussed here might differ depending upon the l values used. This should be borne in mind throughout the paper.

3.2 Model of mixed source

Here, we wish to investigate the effects of varying the relative contributions of the different derivatives. In fact, we shall consider profiles calculated from mixtures of G_Ψ and its first derivative, dG_Ψ/dr, only. The ambiguity of isolating the individual contributions of successive even (or odd) derivatives bears on our decision not to consider higher-order terms. In simple parlance, profiles constructed from G_Ψ look similar to those made from its second derivative, d^2G/dr^2 (which corresponds to the next "even" derivative). The same is true of the first two odd-derivatives.

The manner in which successive even (or odd) derivatives combine with each other depends upon the number of sign changes that take place in making each derivative. If both terms carry the same sign then a linear combination of the two will increase the contribution of the un-normalized, total even (or odd) term to the overall profile (where the latter may be composed of contributions from both even *and* odd terms); if of opposite sign, combining them will reduce it. However, both possibilities will result in an un-normalized, even (or odd) term that has the same shape. Therefore, we cannot gauge the extent to which successive even (or odd) derivatives contribute to the total even (or odd) term. As such we can only make clear statements regarding the relative contributions of the effective, *overall* even and odd terms to the final profile. So, we define our composite, δ-function source according to the linear combination of two terms only, i.e.;

$$\mathcal{S}_\Psi = \epsilon\widetilde{G}_\Psi - (1-\epsilon)(\widetilde{d G_\Psi/dr}) \tag{8}$$

where ϵ is some real, fractional coefficient which controls the mixture, and the tilde above each of the constituent elements indicates that the re-normalized functions are used to make the combination. In order to illustrate the effect of altering ϵ, we begin by considering some modelled profiles.

In Fig. 1, we show the constituent elements of the re-normalized resonant profile (solid line, in power) generated from a δ-function source characterized by G_Ψ alone, i.e., for $\epsilon = 1.0$. The cavity size ($r_a = 3407$ sec) and damping constant (equivalent to a line width in the frequency domain of $\Delta\nu = 1.1\,\mu$Hz) were chosen to mimic the $n = 19$ radial overtone, with frequency $2764.1\,\mu$Hz. These values correspond to those measured in actual low-l helioseismic observations. The real part of G_Ψ is indicated by the dotted line, and the imaginary part by the dashed line (both in amplitude). The source was positioned some 30 sec outside the upper turning point of the cavity, giving rise to a profile with large negative skew symmetry, i.e., with increased power on the low-frequency side of the resonance. It is the vertical displacement, or offset, of the "dispersive" real part that leads to skew symmetry in the combined profile.

We define a measure of the fractional asymmetry of the profile, $\alpha_{\rm skew}$, according to the characteristics of the re-normalized function at the locations where the real part takes its minimum and maximum values (indicated by the shaded vertical bars on the plot), i.e., where the derivatives of the real part are zero. In Fig. 1, the minimum occurs on the low-frequency side: however, this will be reversed for other combinations of cavity characteristics. $P_{\rm low}$ and $P_{\rm high}$ are the re-normalized heights, in power (cf. Equation 7), of the combined profile at the low and high-frequency turning points respectively. These are indicated in Fig. 1. The fractional skewness measure is then simply:

† Source location relative to the base of the photosphere, which is defined where optical depth reaches unity at a wavelength of 500 nm. Throughout the paper, negative values imply a location in the convection zone.

$$\alpha_{\rm skew} = \frac{(P_{\rm high} - P_{\rm low})}{2}. \quad (9)$$

Equation 9 therefore satisfies the definition that negative asymmetry implies elevated power on the low-frequency side of the resonant profile.

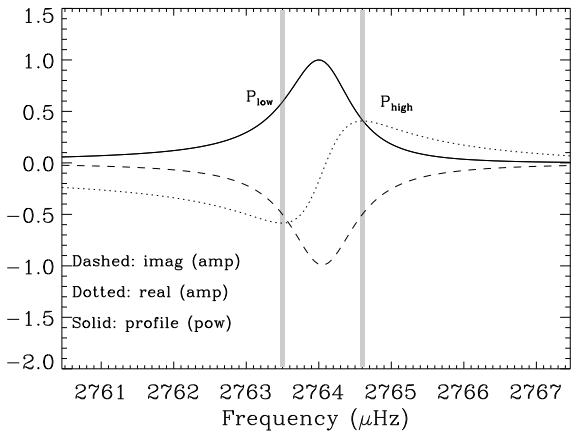

Figure 1. The constituent elements of the re-normalized resonant profile (solid line, in power) generated from a δ-function source characterized by G_Ψ alone. The cavity size ($r_a = 3407$ sec) and damping constant (equivalent to a line width in the frequency domain of 1.1 μHz) have been chosen to mimic an $n = 19$ radial mode with frequency 2764.1 μHz. The real part of G_Ψ is indicated by the dotted line, and the imaginary part by the dashed line (both in amplitude). The source was positioned some 30 sec outside the upper turning point of the cavity, giving rise to a profile with large negative skew symmetry, i.e., increased power on the low-frequency side of the resonance. The real part takes its minimum and maximum values at the locations indicated by the shaded vertical bars; the corresponding power levels in the combined profile are $P_{\rm low}$ and $P_{\rm high}$.

The upper four panels of Fig. 2 show the variation of $\alpha_{\rm skew}$ as a function of the source position d_s, for the same modelled $n = 19$ cavity. We do so for two types of source at four different multipole mixtures ϵ. The dotted line in each panel indicates the skewness for a source characterized solely by G_Ψ, i.e., for $\epsilon = 1.0$; while the solid line shows the skewness for a source characterized by the value of ϵ displayed above each panel. The horizontal dot-dashed line in each plot indicates the skewness, $\alpha_{\rm skew}$, extracted by fits to this mode in the real BiSON data (Chaplin & Appourchaux 1999). Chaplin & Appourchaux fitted a long BiSON spectrum to a model with $\epsilon = 1.0$. They found that for $n > 17$, the fitted d_s showed little variation, and could be fitted to a simple straight-line-offset model with mean ~ -10.5 sec. (Note that the mode asymmetries in the BiSON spectrum are negative, i.e., with more power on the low-frequency side of the resonance.) The skewness of the mode is a fixed observational parameter in a solar p-mode spectrum: however, as indicated by the plots, similar values can be produced by varying both d_s and ϵ.

The fractional skewness has a repeat period corresponding to the nodal separation of the cavity. The calculated $\alpha_{\rm skew}$ for the extreme mixtures with $\epsilon = 1.0$ and 0.0 are out of phase by half the nodal separation. Where the skewness changes sign across a node (or antinode), the imaginary part of function is greatly suppressed (completely so at the node), and the resulting profile no-longer appears "Lorentzian" like. This transition region is quite sharp at most ϵ; however, at $\epsilon = 0.5$ it is very extended, as indicated by the shaded areas on the middle left-hand panel.

The plotted $\alpha_{\rm skew}$ curves may cross the horizontal dot-dashed line – which denotes the measured skewness of this mode in the BiSON data – at one or more locations for a given mixture. Provided these locations give rise to valid, Lorentzian-like resonances of the cavity, they will then correspond to potential estimates of d_s which satisfy the observations. That is, they will give a resonant profile: (i) whose appearance is of the near Lorentzian-like form displayed by the observations; and (ii) whose skewness matches that of the observed profile. The lower left-hand panel of Fig. 2 plots the position of these valid locations in the upper 200 sec of the cavity, for different values of the multipole mixture coefficient ϵ. Once more, we stress that the implied source location is not unique – similar levels of asymmetry recur throughout the cavity. Several locations of d_s may satisfy the observational constraints imposed by the BiSON data at a given ϵ. However, as we go on to discuss below, there is good reason to believe that the favoured source location lies close to the UTP.

When $\epsilon > 0.5$, two locations satisfy the observed-asymmetry constraint: a shallow, near-surface solution, and a second that lies appreciably deeper. Here, we are more interested by the shallower location: as ϵ decreases toward 0.5, so d_s moves progressively higher – and eventually outside – the cavity as a larger fraction of the first derivative dG_Ψ/dr is mixed into the composite source. This can be understood as follows: the first-derivative source gives rise to a positive skewness when d_s lies close to the outer bound of the cavity (see panel for $\epsilon = 0.0$); however, the composite source must act to generate a mode with a negative skewness in order to match the BiSON data. Therefore, as ϵ decreases, the implied source location must move further out to where G_Ψ gives rise to an increasingly negative skew-symmetric contribution (which compensates accordingly).

For $\epsilon < 0.5$, the contribution from dG_Ψ/dr now dominates the composite profile. Since the constraint of generating a negative asymmetry still holds, there must be a jump in the implied source location. For the extreme cases with $\epsilon = 0.0$ and 1.0 (upper left-hand panel) d_s must move deeper by half the nodal separation. For $0.0 < \epsilon < 0.2$, there are in fact three locations which give the required skewness; as ϵ increases still further only the deepest solution remains.

The relative source locations in the lower left-hand panel of Fig. 2 have been converted to implied absolute heights beneath the base of the photosphere (defined where optical depth reaches unity at 500 nm). To do this, we have used the cavity acoustic potential determined from a solar model (model 'S' of Christensen-Dalsgaard et al. 1996) in order to relate the outer bound of the simulated $n = 19$ radial-mode cavity to a physical height in the outer atmosphere of the Sun. (Note that the solar model is normalized to unity radius where $T = T_{\rm eff}$; this height lies some ~ 50 km above our chosen radial datum.) The calculated depths are shown in the lower right-hand panel; the horizontal line indicates the location of the UTP of the $n = 19$ radial mode cavity.

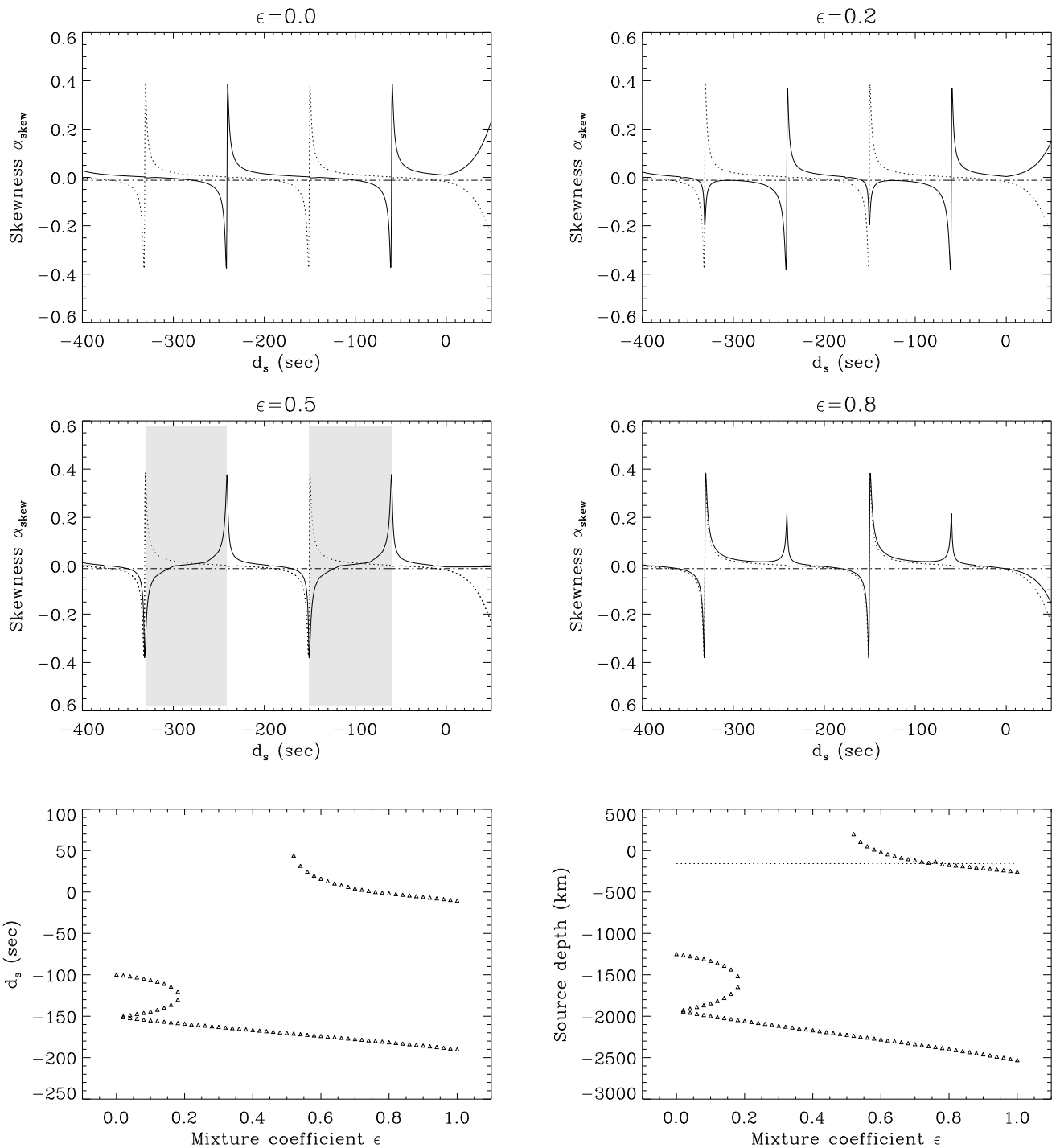

Figure 2. Upper four panels – variation of the fractional skewness, $\alpha_{\rm skew}$, as a function of source depth, d_s, for a modelled mode cavity. The cavity size ($r_a = 3407\,$sec) and damping constant (equivalent to a line width in the frequency domain of $1.1\,\mu$Hz) have been chosen to mimic an $n = 19$ radial mode with frequency $2764.1\,\mu$Hz. Each panel shows the calculated skewness for two types of source at different multipole mixtures ϵ. The dotted line in each panel indicates the skewness for a source characterized solely by G_Ψ, i.e., for $\epsilon = 1.0$; while the solid line shows the skewness for a source characterized by the value of ϵ indicated above each panel. The horizontal dot-dashed line in each plot indicates the observed skewness of this mode ($\alpha_{\rm skew} = -0.017$) inferred from the analysis of BiSON data. Where the skewness changes sign across a node (or antinode), the imaginary part of function is greatly suppressed (completely so at the node), and the resulting profile no-longer appears "Lorentzian" like; at $\epsilon = 0.5$ this region is very extended, as indicated by the shaded areas on the middle left-hand panel. Estimates of d_s which satisfy the observational constraints imposed by the BiSON data lie at the locations where each skewness curve crosses the horizontal dot-dashed line. We only consider these solutions to be valid if they give rise to a Lorentzian-like resonance. The lower left-hand panel plots the position of these valid locations in the upper 200 sec of the cavity, as a function of the multipole mixture coefficient ϵ. Lower right-hand panel – implied absolute locations beneath the base of the photosphere of the relative source depths shown in the lower left-hand panel. The horizontal line indicates the location of the upper turning point of the $n = 19$ radial mode cavity.

Theories of the excitation of the solar p modes by turbulence favour a location for the source in the upper few-hundred kilometers of the convection zone. This appears to be re-enforced by the observation of individual seismic events as cool down-drafts in the inter-granular lanes (Rimmele et al. 1995; Espagnet et al. 1996; Goode et al. 1998) and the complex simulations of Stein & Nordlund (1998a, b). Clearly then, this would tend to favour a lower limit to the mixture coefficient of $\epsilon > 0.5$, with the source locations given by the shallow, near-surface solutions. In an attempt to discriminate further, we now go on to fit the mixed-derivative model to real helioseismic data.

3.3 Fits to a 32-month BiSON spectrum

We have fitted the modes in a 32-month BiSON power spectrum – generated from full-disc Doppler velocity observations made over the period 1994 May 16 to 1997 Jan 10 – to the composite-source model in order to extract estimates of the source depth d_s for different fixed input values of the multipole mixture coefficient. We varied the latter over the range $0.55 \leq \epsilon \leq 1.00$.

Each resonant peak in the frequency domain was modelled according to Equations 7 and 8. We used a multidimensional direction-set minimization algorithm (Press et al. 1992) to fit adjacent $l = 2/0$ pairs in the spectrum by maximizing a log-likelihood function commensurate with the assumed negative exponential statistics in the frequency domain. The following parameters were varied iteratively until they converged to their best-fit values:

(i) A cavity travel time, r_a, for each mode in the pair. The first-guess cavity time was chosen to be appropriate to the radial overtone number of each mode, n.

(ii) A single parameter describing the relative source position d_s, i.e., this was assumed to take the same value for each mode in the pair. This is a valid approximation, since the properties of the modes in the near surface layers are essentially independent of angular degree for $l < 100$. For this reason – in addition to encouraging stability in the fits by keeping the number of freely varying parameters to a minimum – we have fitted a single parameter only.

(iii) A single parameter describing a symmetric rotational splitting pattern for each mode (not applicable to radial modes). For $n > 24$ the rotational splitting pattern was fixed for all modes, with a constant synodic spacing (appropriate to $\Delta|m| = 1$) of 400 nHz (equivalent to a sidereal splitting of ~ 432 nHz).

(iv) A single width for the pair (i.e., all m components in the pair were assumed to have the same width).

(v) A single height – that of the outer, sectoral m components – for each mode. The relative m-component height ratios were assumed to take fixed values (Christensen-Dalsgaard 1989).

(vi) A single relative sideband height for each mode (in order to take account of leakage due to the presence of quasi-periodic dataset gaps in the time domain).

(vii) A flat, background offset for the whole fit.

The natural logarithm of the amplitude, width and background terms were varied – not the straight forward parameters themselves – in order to give a quasi-normal fitting distribution (Toutain & Appourchaux 1994). Estimates of the formal uncertainties in each parameter were then determined from the inverse of the Hessian matrix describing the hyper-surface of the fit.

Table 1. Mean location of the excitation source, in kilometers beneath the base of the photosphere (defined where optical depth reaches unity at 500 nm), as a function of the multipole mixture coefficient ϵ. Each entry is the weighted mean over locations inferred from fits to the BiSON power spectrum which cover the radial order range $12 \leq n \leq 28$.

Mixture coefficient ϵ	*Mean source location* (km)
0.55	135 ± 17
0.60	23 ± 16
0.70	-81 ± 16
0.80	-140 ± 14
0.90	-176 ± 15
1.00	-221 ± 17

The upper panel of Fig. 3 shows the fitted relative source positions d_s as a function of the overtone number, n, of the radial mode in each fitted pair for different input values of ϵ. Negative values of d_s imply that the source lies inside the bounded cavity. The formal uncertainties which we show for $\epsilon = 1.0$ only are also representative of those for the other source mixtures.

The relative source locations in the upper panel of Fig. 3 have been converted to absolute heights beneath the base of the photosphere, once more through the use of model 'S' of Christensen-Dalsgaard et al. (1996). The implied absolute depths are shown in the lower panel of the figure – the solid line on the plot follows the location of the UTP of the resonant cavity for radial modes. The (weighted) mean source location over the range $12 \leq n \leq 28$ is shown in Table 1 for each value of the mixture coefficient ϵ.

3.4 Discussion

First, we ask whether it is possible to discriminate between the various ϵ on the basis of the quality of the fits. This can be done by comparing the maximized logarithmic-likelihood functions returned by fits at the same n (Appourchaux, Gizon & Rabello-Soares 1998). We find that the logarithmic likelihoods of analogous fits agree typically to within ≈ 0.01; further, there is no clear, repeated trend in the pattern of the differences as a function of ϵ. We are therefore forced to conclude that is it extremely difficult to select a preferred mixture coefficient on the basis of such a comparison. As such, we must bring other independent information to bear in our efforts to constrain ϵ.

As noted previously, direct observations of acoustic events located in the cool, intergranular lanes, and simulations of convection both appear to favour a location for the excitation in a thin layer just beneath the photosphere. The turbulent pressure has a sharp maximum in the superadiabatic layer of the convective zone, peaking some ~ 75 km beneath the base of the photosphere. Stein & Nordlund (1998a,

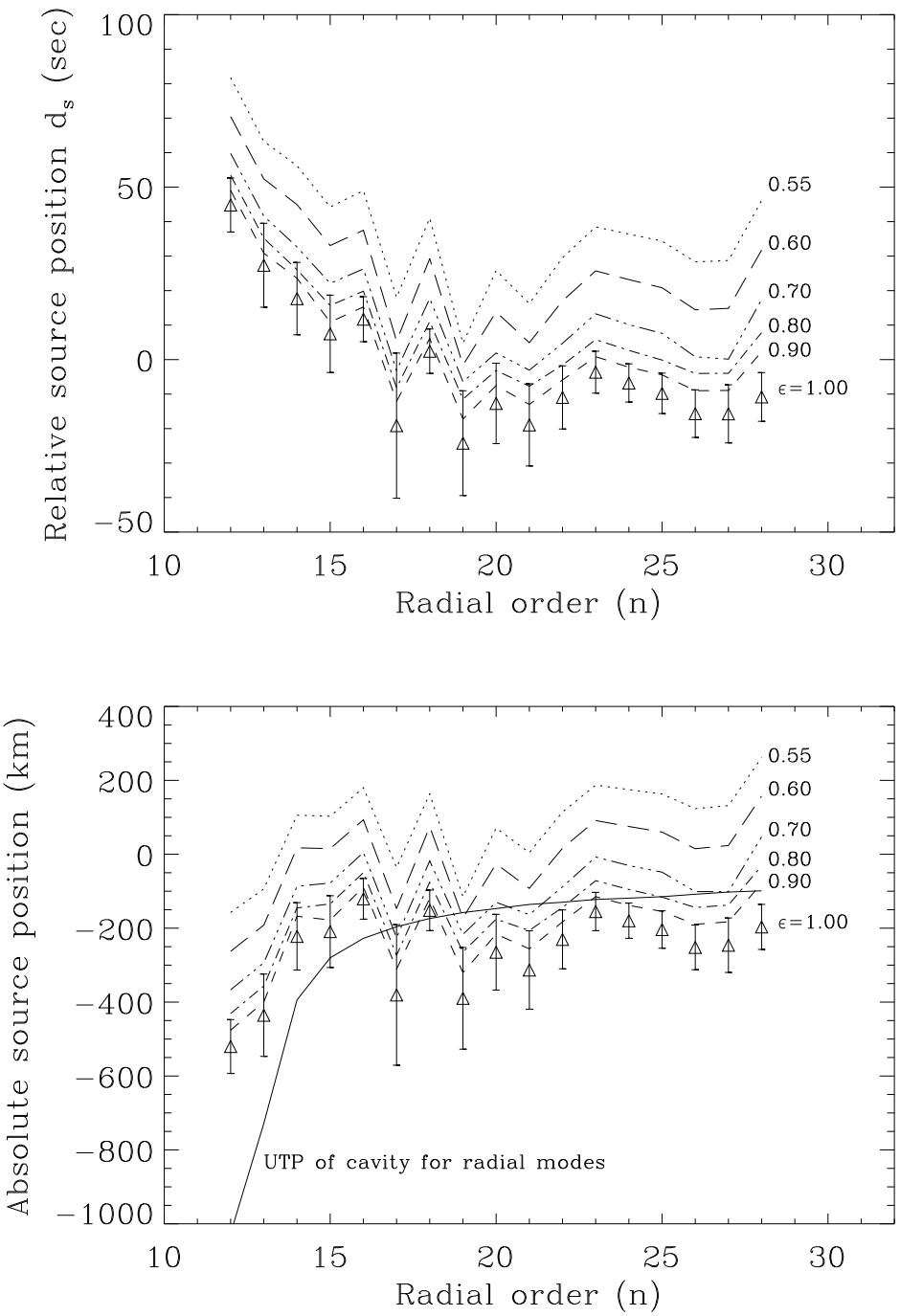

Figure 3. Results of fitting modes in a 32-month BiSON power spectrum for the source location. Upper panel – Fitted relative source position, d_s (in seconds of travel time), plotted as a function of the overtone number, n, of the radial mode in each fitted pair for different input values of the multipole mixture coefficient ϵ (see annotation on plot). Negative values of d_s imply that the source lies inside the resonant cavity. The plotted error bars – which we show for $\epsilon = 1.0$ only – are the formal uncertainties derived from the Hessian of each fit; they are representative of those returned for the other mixtures. Lower panel – Implied absolute locations, in kilometers beneath the base of the photosphere (defined where optical depth reaches unity at 500 nm), of the fitted estimates in the upper panel. The solid line follows the location of the upper turning point of the resonant cavity for radial modes.

b) performed complex, 3-dimensional simulations of convection, and considered the excitation of acoustic modes via non-adiabatic gas-pressure, or entropy, fluctuations which were found to be localized principally in the cool, intergranular lanes of the evolving models. They found that for the strongest modes, the integrand of the work integral which describes the driving of the resonances was peaked strongly in the superadiabatic boundary layer at a depth of ~ -70 km. (This is not necessarily the case for lower-frequency modes; see below in Section 4.3.)

The key inference to be drawn from Fig. 3 and Table 1 is that in order to give a shallow source location of less than -100 km, we require $0.73 > \epsilon > 0.50$, i.e., there must be an appreciable fraction of the odd-derivative present in the source mixture. As ϵ is increased, so the estimated source locations move deeper. Interestingly, Vorontsov et al. (1998) found that a mixed source, located close to the photosphere, was required in order to match the high-frequency phenomenon observed in the South Pole data which arises from interference occurring in the layer between the source and UTP.

At all ϵ, we find suggestions of a slight n dependence in the inferred location, with lower-frequency modes excited at a slightly greater depth. This is what one might expect on the basis of the stratification of eddy scales with height (i.e., deeper-lying, larger-scale eddies couple more strongly to low-frequency modes). Above $n \approx 16$, the fitted d_s show little variation, given the uncertainties on the data. There is perhaps a slight indication that for lower values of ϵ, the trend is not as flat and shows indications of a small positive gradient above $n = 16$; however, given the uncertainties on each datum, this is once more not significant. As ϵ decreases toward 0.5, so these locations eventually become evanescent; in fact, the mean d_s computed over the range $17 \leq n \leq 28$ becomes positive for $\epsilon < 0.79$.

Thus far we have considered the source to be a δ-function in the radial direction. A more-realistic model will consist of suitably weighted contributions from a range of radii near the top of the convection zone. We therefore now go on to assess the impact of an extended source.

4 RADIAL EXTENT OF THE SOURCE

4.1 Model of extended source

In the spirit of Abrams & Kumar (1996), for simplicity we describe the strength of our extended source in terms of a Gaussian distribution of width Δ_s in the radial direction, centered on r_s^c, such that its relative location is given by:

$$d_s^c = r_s^c - r_a.$$

The contribution of the composite source at radius r is:

$$s_\Psi(r) = [\epsilon \widetilde{G}_\Psi - (1-\epsilon)(d\widetilde{G_\Psi}/dr)] \exp\left(-(r-r_s^c)^2/2\Delta_s^2\right). \quad (10)$$

The total profile, $\mathcal{S}_\Psi$ follows by integrating the contributions over all r, i.e.,

$$\mathcal{S}_\Psi = \int_r s_\Psi(r) dr. \quad (11)$$

In practice, we implement Equation 11 by performing a linear summation of the contributions s_Ψ at discrete locations across the range $r = r_s^c \pm 4\Delta_s$, i.e.,

$$\mathcal{S}_\Psi = \sum_{r=r_s^c-4\Delta_s}^{r=r_s^c+4\Delta_s} s_\Psi(r). \quad (12)$$

The above assumes that the radial distributions are similar for different multipoles, which may not be the case in reality; however, this does avoid added complexity both in the simulations and in interpreting the results.

4.2 Effect of source width for fixed mode skewness

In Fig. 4 we show the change in the inferred location of the source (now its peak location d_s^c) as its width Δ_s is increased incrementally to ~ 25 sec. In the near-surface layers of the convection zone, this corresponds to a geometric width of ~ 250 km; the $\pm 4\Delta_s$ range therefore extends over some ~ 2000 km. We again illustrate results for multipole mixture coefficients which cover the range $0.55 \leq \epsilon \leq 1.00$, and for three simulated radial-mode cavities: the $n = 12$ overtone, with cavity size $r_a = 3264$ sec and damping equivalent to a linewidth of $\Delta\nu = 0.28\,\mu$Hz; the $n = 19$ overtone, with $r_a = 3407$ sec and $\Delta\nu = 1.11\,\mu$Hz; and the $n = 26$ overtone, with $r_a = 3471$ sec and $\Delta\nu = 4.28\,\mu$Hz. In addition, we have imposed the constraint that at any given n, all constructed profiles must possess the same skewness, $\alpha_{\rm skew}$, corresponding to that of the appropriate radial overtone in the BiSON data. We note also that our "starting" source locations, for $\Delta_s = 1.0$, correspond to the near-surface solutions found in each cavity for $\epsilon > 0.5$ (e.g., as illustrated for $n = 19$ in Fig. 2; the plots look similar at other n). The variation of these as a function of n can be seen in the fits to the BiSON spectrum in Fig. 3.

The results indicate an overall tendency for d_s^c to move deeper as the source width is increased. The detail of each plot depends upon the precise interaction of the extended source and the characteristics of the composite source profile $\mathcal{S}_\Psi$ at the locations covered by the source. These results are clearly only pertinent to a strongly peaked source, as described here. As shown in Fig. 2, the variation of skewness becomes quite complicated in the vicinity of both the nodes and antinodes when we have a mixed multipole source. Inferred changes to the source location therefore depend sensitively upon: whether the source distribution traverses a node or antinode in the radial direction; and the size of the contribution of that part of source that does so. Clearly, the assumed form we adopt for the radial description plays a crucial role.

Our analyses here do not allow us to constrain independently the extent of the source; we can however comment upon the effects of an extended distribution provided we adopt an assumed form for it. Here we have considered the rôle played by source functions that are peaked strongly in a Gaussian manner in the radial direction. To avoid those complications which arise when we have node/antinode traversals, we have further restricted ourselves to the consideration of sources located only in the very near-surface layers – here, Gaussian sources which at most extend over a complete range of roughly ≈ 2000 km.

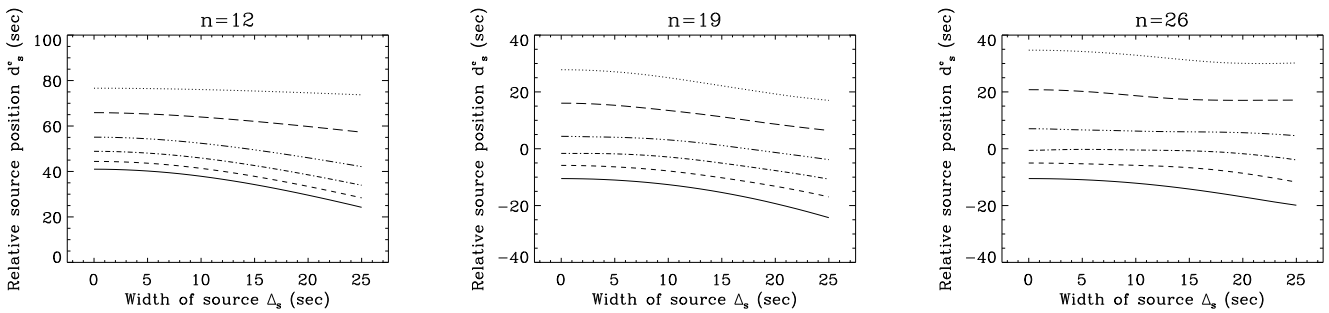

Figure 4. The inferred central location of the extended Gaussian source, d_s^e, as a function of the width of the source, Δ_s, for three different modelled radial-mode cavities: left-hand panel – the $n = 12$ overtone, with cavity size $r_a = 3264$ sec and damping equivalent to a linewidth of $\Delta\nu = 0.28\,\mu$Hz; centre panel – the $n = 19$ overtone, with $r_a = 3407$ sec and $\Delta\nu = 1.11\,\mu$Hz; right-hand panel – the $n = 26$ overtone, with $r_a = 3471$ sec and $\Delta\nu = 4.28\,\mu$Hz. We illustrate results for multipole mixture coefficients 0.55 (upper dotted line on each panel), 0.60, 0.70, 0.80, 0.90 and 1.00 (lower solid line on each panel). At any given n, all constructed profiles have the same skewness, $\alpha_{\rm skew}$, as that of the appropriate radial overtone in the BiSON data.

4.3 Discussion

Kumar (1994) modelled turbulence in the outer layers of the convection zone in the form of critically damped eddies covering a range of different length scales. The resulting source function Kumar constructed – in essence that expected for quadrupolar emission – was peaked strongly at a depth of ~ -60 km, with an approximate half-width of ~ 40 km. Kumar also considered the effects of increasing the radial extent of the source: he found that this reduced the contrast between the peaks and troughs of a simulated model of the high-frequency South-Pole pseudo-mode spectrum. By comparing the modelled data with the observations, he estimated that the acoustic emission appeared to be concentrated in a layer of thickness less than ~ 550 km.

The complex simulations of Stein & Nordlund (1998a, b; see Section 3.4) inferred that the integrand of the work integral which describes the excitation process is peaked strongly in the superadiabatic boundary layer for p modes in the range 3000 to 4000 μHz. The half-width of the principal peak in the integrand is of the order of $\sim$ 100 to $\sim$ 200 km. However, Stein & Nordlund found that the radial distribution of the driving is somewhat more complex than a simple, Gaussian-like function. Indeed, at low frequencies ($\sim 2000\,\mu$Hz) their simulations indicate that the driving occurs at similar levels across a much-greater range of depths – a strongly peaked function would then appear to be an inappropriate choice to describe the source.

In order to interpret the results in Fig. 4, we begin by reminding the reader that the source locations shown are those which satisfy the constraint of giving resonant profiles with asymmetries that match those in the BiSON data, and which correspond to the shallow, near-surface solutions admitted by each simulated cavity.

The results of Fig. 4 show that when the source has width, the implied source locations lie at greater depths. For example, when our Gaussian source has a half-width equivalent to ~ 100 km (about ~ 10 sec) the inferred source locations are depressed by a few seconds at each ϵ. The precise value again depends upon both n and ϵ.

We have already seen that current prejudice favours a location for the source very close to the base of the photosphere. In Section 3, we saw that in order to place the source at a depth of less than ~ -100 km we required $0.73 > \epsilon > 0.50$ when $\mathcal{S}_\Psi$ was constructed from a δ function source. If we are to maintain such shallow, inferred central locations for models constructed with an *extended* source, ϵ must therefore be *decreased* still further. We have estimated the extent to which ϵ must be changed by making use of simulations of the type shown in Fig. 4. We show the results in Fig. 5. Here, we plot the mean required change to the mixture coefficient, $< \delta\epsilon >$, averaged over $12 \leq n \leq 28$; we do so for different "starting" mixtures, ϵ_0. These correspond to the source mixture at source width $\Delta_s = 0$; the plotted curves then show the extent to which this starting mixture must be decreased in order to maintain the same source location, as Δ_s is gradually increased. Fig. 5 shows clearly that the required change to ϵ is greater: (i) at larger starting mixtures, ϵ_0; and (ii) at larger values of Δ_s.

With a starting mixture of $\epsilon_0 = 0.73$ – which gives us a mean source depth of ~ -100 km – we find that the change to the source mixture required to maintain the same mean location is $< \delta\epsilon > \approx -0.014$ (averaged over all n). Clearly, the small size of $< \delta\epsilon >$, and its negative sign, again indicate that our simulations appear to favour a well-mixed source if it is to be placed very close to the surface (and is strongly peaked in those layers).

Because of the results of the simulations of Stein & Nordlund, the extent to which our results are relevant at low n is unclear. As indicated above, the impact made by a very extended source depends critically upon how we define its form. However, interestingly, our results do show some evidence for the expected n dependence in the source location (i.e., lower-frequency modes excited at a slightly greater depth).

5 SOLAR-CYCLE VARIATION OF SKEWNESS PROPERTIES

5.1 Analysis of the BiSON dataset

In an effort to uncover possible changes to the properties of the source over the solar activity cycle, we have analyzed Doppler velocity observations made by BiSON over the period 1991 Jan 1 to 1997 Sep 1. These cover the complete

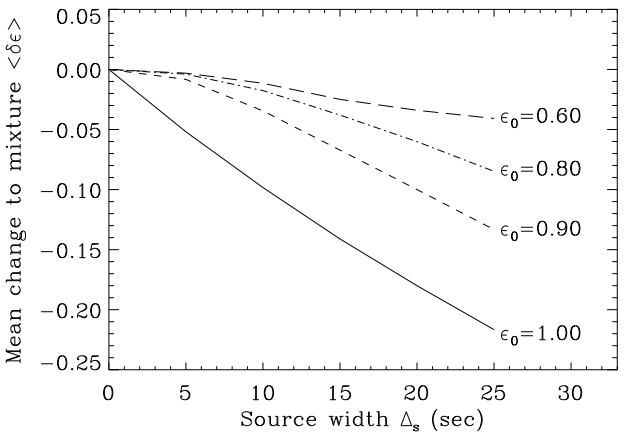

Figure 5. The inclusion in the model of an extended source tends to depress – by several seconds – estimates of the source depth extracted from analyses with a δ-function source. In order to maintain a given source depth, the source mixture coefficient, ϵ, must be decreased in order to compensate. Here, we show the extent to which ϵ must be changed, as averaged over modes in the range $12 \leq n \leq 28$. We do so for different "starting" values of the mixture, as annotated on the plot. These values correspond to the mixture at source width $\Delta_s = 0$; the plotted curves then show the extent to which this starting mixture must be depressed in order to maintain the same source location, as Δ_s is gradually increased.

declining phase of solar activity cycle 22, from an activity maximum through to the minimum at the cycle 22/23 boundary.

We divided the dataset in two ways. We began by constructing two 32-month time series, the first made from data collected over the period 1991 Jan 1 through 1993 August 23 (at high activity), and the second from observations made between 1994 May 16 and 1997 Jan 10 (low activity). We determined the mean, smoothed 10.7-cm radio flux (in RF units) over the period of both sets of observations. (Note that 1 RF unit corresponds to $10^{-22}\,\mathrm{W\,m^{-2}\,Hz^{-1}}$.) This measure serves as our proxy of the level of solar activity. We find mean levels of ~ 165 and ~ 76 RF units respectively – these are to be compared with the notional minimum activity level of 65 RF units. We also constructed 10 8-month contiguous time series, which cover the full epoch indicated above; the mean flux levels encountered over these time periods range from ~ 72 to ~ 220 RF units.

We fitted peaks in the power spectra generated from these data strings to both the mixed-derivative model, with $\epsilon = 1.0$ (see below), and a polynomial skew-symmetric formalism derived by Nigam & Kosovichev (1998b). (For a description of the use of this fitting formalism with low-l data, see Toutain et al. 1998; Chaplin et al. 1999.) The effects of skew symmetry appear explicitly as a single parameter in the formalism. Fitted estimates of the parameter, B_{skew}, provide a measure of the fractional asymmetry of the modes. For a given cavity and source combination, estimates of B_{skew} are quantitatively similar to our estimate, α_{skew}.

An estimate of any solar-cycle changes based upon the level of asymmetry of the modes is appealing, since this measure is a fixed characteristic of any peak in any spectrum; this is not the case for estimates of d_s, as we have seen throughout the paper. Here, we therefore restrict ourselves to considering a single mixture (i.e., $\epsilon = 1.0$), but discuss the impact that changes to, for example, the multipole mixture or source width have on the results.

For the 32-month spectra, we simply compared the fitted estimates of d_s and B_{skew} at each n accordingly. However, we performed a slightly more involved analysis on the two sets of parameters extracted by the 8-month fits. At each (l, n), we constructed a mean dataset from a weighted average of the parameter estimates (i.e., either d_s or B_{skew}) from those spectra made from data collected at low levels of activity. We used the formal uncertainties returned by the fitting procedure to fix the weights. Difference residuals were then calculated – with respect to the values in the average set – for each datum in each spectrum. Separate linear fits were then made, again at each (l, n), between: the 10 parameter residuals; and the 10 corresponding values of the mean 10.7-cm radio flux (in RF units) observed over the duration of the time series used to generate each spectrum. The returned best-fit gradients from the linear fits were then a measure of the observed change in the parameter per unit change in activity (here, per unit RF); if multiplied by the extreme change to the 10.7-cm flux over the solar cycle, they correspond to the implied activity minimum-to-maximum change in the parameter. (Our analyses assume a linear dependence with activity. We justify this by noting that the precision in these fitted parameters is such that the use of higher-order functions for parameterizing the variations is inappropriate.)

5.2 Results and discussion

When we compare the fitted d_s and B_{skew} for both dataset lengths, we find no evidence for any significant changes to these parameters over the solar cycle, either individually as a function of n, or when they are averaged over several radial orders in an effort to reduce the associated uncertainties. Given the inherent precision in the parameters, we can therefore only set upper limits to any long-term activity-related variations.

Over the range $15 \leq n \leq 25$, our analyses place an upper limit to any fractional increase in the magnitude of the asymmetries – from solar minimum to maximum – of $\delta B_{\mathrm{skew}}/B_{\mathrm{skew}} \sim 27 \pm 25$ per cent (1σ), i.e., a positive value here implies the asymmetries become more negative. Fits to a model based on $\mathcal{S}_\Psi$ with $\epsilon = 1.0$ give an upper limit to any *implied* absolute increase to the source location – again averaged over n – of $\delta d_s = 8.3 \pm 7.1$ sec (1σ), i.e., a positive value for δd_s implies a shallower source location. We emphasize that this is only an implied upper limit, since variations to d_s apparently uncovered by the fits could be explained in one of several different ways. We consider a few possibilities in turn.

5.2.1 Changes to the source location and width, and the cavity UTP

Our fits provide a direct estimate of the location of the source *relative* to the UTP of the resonant cavity; changes to d_s would therefore arise were the cavity dimensions to

change at the UTP, while the absolute location of the excitation source remained fixed in the upper layers of the convection zone. The modal eigenfrequencies increase by at most $\sim 0.4\,\mu$Hz from activity minimum to maximum (e.g., Elsworth et al. 1990; Libbrecht & Woodard 1990, 1991; Regulo et al. 1994; Elsworth et al. 1994; Chaplin et al. 1998); were these variations to arise solely from changes to the cavity size, we might then expect to uncover changes to d_s of at most ~ 0.4 sec. This is at a level well below our 1-σ upper limit.

An actual change in the central location of the source of ~ 7 sec (our rough 1σ estimate) corresponds to a geometric change of ~ 70 km. Changes to the implied source location could also arise from variations in the radial extent of the source. As discussed in Section 4.3, assessing the size of this effect is quite complex, and depends in detail upon the assumed characteristics of the source (including the multipole mixture ϵ), and its precise interaction with the cavity. With reference to Fig. 4, for some combinations of n and ϵ, a change in the radial extent of the source of a few seconds would suffice to explain the 7-sec change in d_s; however, for others, much-larger implied variations in Δ_s, of the order of 20 sec or more, are required. These upper-limit distance scales would imply major structural alterations in the superadiabatic layer.

5.2.2 Changes in the source multipole mixture

As indicated by the results in Section 3 variations in ϵ will give rise to changes in the implied source location.

We have used results from both simulations and from fits to the BiSON spectra to establish the size of the implied change to the multipole mixture coefficient, $\delta\epsilon$, that could give rise to our upper limit in δd_s. As evidenced from the fitted data plotted in Fig. 3, the relationship between d_s and ϵ is non-linear. With a starting mixture close to $\epsilon \sim 1.0$, we find that the decrease (again averaged over n) required to give the upper limit in δd_s is $\delta\epsilon \sim -0.23 \pm 0.20$; with a starting mixture of $\epsilon \sim 0.73$, its implied magnitude is reduced to $\sim -0.07 \pm 0.06$. With ϵ close to 0.55, $\delta\epsilon$ reduces still further to $\sim -0.04 \pm 0.03$.

5.2.3 Correlated contribution from granulation

Our analyses in this paper have been framed under the assumption that Doppler velocity observations of the acoustic resonances are unaffected by any correlated contribution from the granulation. While most treatments of this topic follow the same convention (e.g., see Nigam & Kosovichev 1999a, b; Kumar & Basu 1999a; and Chaplin & Appourchaux 1999), the assumption of a lack of any contribution at all is open to question. The presence of some small component in the velocity observations, whose size changed over the solar cycle, would also alter our estimates of d_s accordingly – this is because variations to the correlated granular noise would lead to alterations in the form of the observed resonant profiles.

Chaplin & Appourchaux (1999) followed simple reasoning based upon the relative sizes of acoustic and convective motions observed in Doppler velocity and intensity observations to show that one might expect the correlated contribution in intensity to be ≈ 5 times larger (in amplitude) than that in velocity. Further, they went on to measure the fractional amplitude (relative to the radial p-mode amplitudes) of the component in VIRGO/SPM intensity data, and found that at blue wavelengths it varied from ~ 2 to ~ 5 per cent. A simple scaling argument might then imply upper limits to the contribution in velocity of less than 1 per cent.

We have performed a series of simulations with modelled sources, to which we have added a simple offset to represent the correlated noise. The addition of the extra component in the complex domain shifts the real, dispersive part of the source function and as a result modifies the observed form of the resonant profile. We find that a fractional component of size ~ 0.5 per cent typically shifts the implied source location by our 1-σ limit of 7 sec. This is also of a similar size to our rough upper-limit estimate of the size of any correlated noise present in the Doppler velocity observations. Since the implied shift in d_s that results from the introduction of such a component – again, of the order of 7 sec – is at a level below the size of the uncertainties on those estimates of d_s extracted from fits to the BiSON data, our assumption of a complete lack of any contamination in Doppler velocity is not unreasonable given the inherent precision in the data.

6 SUMMARY

We have investigated various properties of the excitation source that is responsible for driving the acoustic p-mode oscillations of the Sun. In particular, we have considered in detail how the precise nature of the resonant mode spectrum is modified: (i) as a result of the impact of different source multipole mixtures; and (ii) as a function of the radial extent of the source. To do this, we have modelled the observed resonant spectra with the solutions to a simple, one-dimensional wave equation which is intended to describe the essential elements of the solar resonant acoustic cavity. These are constructed from the Green's function, G_Ψ, of the wave equation and it's first derivative, dG_Ψ/dr. Further, we have also fitted these models to the low-l peaks in a high-resolution power spectrum generated from data collected by the Birmingham Solar-Oscillations Network (BiSON).

We investigated mixed-multipole δ-function sources constructed from a linear combination of the zeroth (even term) and first (odd term) derivatives of G_Ψ. We find that in order to place the source in the upper few-hundred kilometers of the convection zone, the even term must contribute at least 50 per cent of the source mixture; further, if the source is restricted to lie within ~ 100 km or so of the base of the photosphere, a well-mixed source is required (with the odd term contributing roughly ≈ 27 per cent to the admixture). When the source is constructed from the even term only, its inferred location lies at a greater depth, some ~ 221 km beneath the top of the convection zone.

We have also modelled extended sources, whose distribution is described by a Gaussian in the radial direction. We have only considered sources whose radial extent is restricted to the upper ≈ 1000 km or so of the convection zone; the inclusion in the model of an extended source tends to depress – by several seconds – estimates of the source depth extracted from analyses with a δ-function source. Therefore,

in order to maintain a given source depth, a still-greater proportion of the odd derivative must be present in the source admixture. Consequently, these results also favour a well-mixed source if it is to be placed very near the surface.

Finally, we have also used the extensive BiSON dataset to search for variations in the source characteristics over the solar cycle. The inherent precision of the data is such that we can only place upper limits on changes to the skewness properties of the modes. Over the range $15 \leq n \leq 25$, our analyses place an upper limit to any fractional change in the magnitude of the fitted asymmetries – from solar minimum to maximum – of $\delta B_{\rm skew}/B_{\rm skew} = 27 \pm 25$ per cent (1σ), i.e., a positive value here implies that the asymmetries become more negative. We have also estimated the upper limit to any change in the fractional contribution from the even derivative of the multipole mixture. Care must be taken in attempting to extract this estimate, since its implied magnitude is a non-linear function of the mixture of the source. When the even derivative contributes most of the source mixture, we find an upper limit of $\sim -0.23 \pm 0.20$ (1σ); when the odd derivative contributes nearly half of the admixture, this reduces to $\sim -0.04 \pm 0.03$.

ACKNOWLEDGMENTS

This work utilizes data collected by the ground-based Birmingham Solar-Oscillations Network (BiSON). We would like to thank H. K. Williams, J. Litherland and J. Allison in Birmingham; P. Fourie at SAAO: and our hosts R. Stobie (SAAO); the Carnegie Institution of Washington; the Australia Telescope National Facility (CSIRO); E. J. Rhodes (Mt. Wilson, California); and the IAC, Tenerife. BiSON is funded by the UK Particle Physics and Astronomy Research Council. WJC acknowledges the support of an ESA Internal Fellowship. We thank D. Gough and J. Christensen-Dalsgaard for helpful discussions, and T. Sekii for providing the modelled solar acoustic potential

REFERENCES

Abrams D. & Kumar P., 1996, ApJ, 472, 882
Appourchaux T., Chaplin, W. J., Elsworth, Y., Isaak, G. R., McLeod, C. P., Miller, B. A. & New, R., 1998, in: Proc. IAU Symp. 185 'New Eyes to See inside the Sun and Stars. Pushing the Limits of Helio- and Asteroseismology with New Observations from Ground and from Space', ed. Deubner F.-L., Kluwer, Dordrecht, p. 45
Appourchaux T., Gizon L. & Rabello-Soares M. C., 1998, A&AS, 132, 107
Chaplin W. J., Elsworth Y., Isaak G. R., Lines R., McLeod C. P., Miller B. A. & New R., 1998, MNRAS, 300, 1077
Chaplin W. J. & Appourchaux T., 1999, MNRAS, in press
Chaplin W. J., Elsworth Y., Isaak G. R., Miller B. A. & New R., 1999, MNRAS, in press
Christensen-Dalsgaard J., 1989, MNRAS, 239, 977
Christensen-Dalsgaard J., et al., 1996, Science, 272, 1286
Christensen-Dalsgaard J., Rabello-Soares M. C., Rosenthal C. S. & Thompson M. J., 1998, in 'SOHO6/GONG98 Workshop: Structure and dynamics of the interior of the Sun and Sun-like stars', eds. Korzennik S. & Wilson A., ESA SP-418, p. 147
Duvall T. L., Jefferies S. M., Harvey J. W., Osaki Y. & Pomerantz M. A., 1993, ApJ, 410, 829
Elsworth Y., Howe R., Isaak G. R., McLeod C. P., & New R., 1990, Nature, 345, 322
Elsworth Y., Howe R., Isaak G. R., McLeod C. P., Miller B. A., New R., Speake C. C. & Wheeler S. J., 1994, ApJ, 434, 801
Espagnet O., Muller R., Roudier Th., Mein N., Mein P. & Malherbe J. M., 1996, A&A, 313, 297
Fröhlich C. et al., 1997, Sol. Phys., 170, 267
Gabriel M., 1995, A&A, 302, 271
Goldreich P. & Kumar P., 1990, ApJ, 363, 694
Goode P. R., Strous L. H., Rimmele T. R. & Stebbins R. T., 1998, ApJ, 495, L27
Korzennik S. G., 1998, in 'SOHO6/GONG98 Workshop: Structure and dynamics of the interior of the Sun and Sun-like stars', eds. Korzennik S. & Wilson A., ESA SP-418, p. 933
Kumar P., 1994, ApJ, 428, 827
Kumar P. & Basu S., 1999a, ApJ, 519, 389
Kumar P. & Basu S., 1999b, ApJ, 519, 396
Libbrecht K. G. & Woodard M. F., 1990, Nature, 345, 779
Libbrecht K. G. & Woodard M. F., 1991, Science, 253, 152
Lighthill M. J., 1952, Proc. Roy. Soc. London A., 211, 564
Nigam R., Kosovichev A. G., Scherrer P. H. & Schou J., 1998, ApJ, 495, L115
Nigam R. & Kosovichev A. G., 1998, ApJ, 505, L51
Nigam R. & Kosovichev A. G., 1999, ApJ, 510, L149
Nigam R. & Kosovichev A. G., 1999, ApJ, 514, L53
Press W. H., Teukolsky S. A., Vetterling W. T. & Flannery B. P., 1992, in: Numerical Recipes in Fortran (Second Edition), Cambridge University Press, Cambridge, p. 407
Rast M. P. & Bogdan T. J., 1997, ApJ, 496, 527
Rimmele T. R., Goode P. R., Harold E. & Stebbins R. T., 1995, ApJ, 444, L119
Regulo C., Jimenez A., Palle P. L., Hernandez F. P. & Cortes T. R., 1994, ApJ, 434, 384
Rhodes E. J. Jr., Kosovichev A. G., Schou J., Scherrer P. H. & Reiter J., 1997, Sol. Phys., 175, 287
Rosenthal C. S., 1998a, ApJ, 508, 864
Rosenthal C. S., 1998b, in 'SOHO6/GONG98 Workshop: Structure and dynamics of the interior of the Sun and Sun-like stars', eds. Korzennik S. & Wilson A., ESA SP-418, p. 957
Roxburgh I. W. & Vorontsov S. V., 1995, MNRAS, 272, 850
Roxburgh I. W. & Vorontsov S. V., 1997, MNRAS, 292, L33
Stein R. F. & Nordlund A., 1998, ApJ, 499, 914
Stein R. F. & Nordlund A., in 'SOHO6/GONG98 Workshop: Structure and dynamics of the interior of the Sun and Sun-like stars', eds. Korzennik S. & Wilson A., ESA SP-418, p. 693
Toutain T. & Appourchaux T., 1994, A&A, 289, 649
Toutain T., Appourchaux T., Fröhlich C., Kosovichev A. G., Nigam R. & Scherrer P. H., 1998, ApJ, 506, L147
Vorontsov S. V., Jefferies S. M., Duvall Jr. T. L. & Harvey J. W., MNRAS, 298, 464